Geomorphology 103 (2009) 130–135

Contents lists available at ScienceDirect

Geomorphology

journal homepage: www.elsevier.com/locate/geomorph

Analysis of massif fracturing during Deep-Seated Gravitational Slope Deformation by physical and numerical modeling

D. Bachmann *, S. Bouissou, A. Chemenda

Géosciences Azur, UMR 6526, Université de Nice-Sophia Antipolis, 250 rue Albert Einstein, 06560 Valbonne, France

ARTICLE INFO

Article history:
Accepted 23 September 2007
Available online 9 May 2008

Keywords:
Deep-Seated Gravitational Slope Deformation
Sagging
Sackung
Fracture
Physical modeling

ABSTRACT

Both 3-D physical modeling and 2-D numerical modeling were used to analyze the development of Deep-Seated Gravitational Slope Deformations. We focused especially on the link between fracturing and morphological features such as Sagging/Sackung. Physical modeling was performed by using properly scaled analogue materials as well as an original vertical accelerator device. This device enables cyclic loading of the model, and to advance step by step in the deformation process. This technique is thus particularly well suited to analyze rupture initiation and evolution. Surface deformation is registered with a high resolution digital camera. Internal model deformation was studied by making cross-sections at different experiment stages. The failure of one or both mountain sides was observed, with a deep-seated failure zone that follows an almost circular trajectory. It intersects the surface perpendicularly in the upper part. Other fractures are generated in the moving mass in response to its motion. Fracture network becomes wider and morphological features such as counterscarps are generated. Numerical models were performed with a 2-D finite element code named Adeli. We tried to reproduce physical modeling results by using the same mechanical behaviour and parameters of the analogue material. The results reproduced failure initiation well, but poorly described moving mass deformation. Furthermore rupture initiation in the 2-D numerical models occurs more easily (e.g. for a lower acceleration value) than in the 3-D physical models, confirming the importance of the three dimensional analysis.

1. Introduction

Deep-Seated Gravitational Slope Deformations (DSGSD) are common in all mountain ranges (Crosta, 1996; Agliardi et al., 2001; Tibaldi et al., 2004). They are observed in a wide variety of lithologies and geomechanical characteristics (McCalpin and Irvine, 1995; Crosta, 1996). Those very deep-seated slow deformations, also called "Sagging" or "Sackung", are characterized by morpho-structural features such as double ridges, ridge top depressions, scarps and counterscarps, trenches, etc. (Zischinsky, 1966; Beck, 1968; Savage and Varnes, 1987; Hutchinson, 1988; Agliardi et al., 2001; Kinakin and Stead, 2005). The link between those morpho-structural features and deformation in the mobilized mass is however not well known. Deep deformation is often considered as a creep phenomenon without a well-defined continuous sliding surface (Zischinsky, 1966; Tabor, 1971; Mahr, 1977; Mahr and Nemcok, 1977; Bisci et al., 1996; Kinakin and Stead, 2005). Nevertheless, some authors consider the possibility of well well-defined single or multiple sliding surfaces crossing the whole mountain if the amount of deformation is large enough (Beck, 1968; Radbruch-Hall, 1978; Crosta, 1996). As counterscarps are often up to 10 m high and slopes are about 1000 m high (McCLeary et al., 1978; McCalpin and Irvine, 1995), the amount of deformation in a DSGSD is commonly of about 0.01. This is an important strain for geological materials, so that it is very unlikely for deformation not to be localized under these conditions. In any case the shape and depth of the failure zone, as well as its relations with morpho-structural features are not well-constrained. Such knowledge is also important from a hazard mitigation point of view. Indeed, many mass movements occurring at smaller time- and spatial-scale are observed in rock masses already affected by DSGSD (Bisci et al., 1996; Crosta, 1996; Agliardi et al., 2001). However, the link between those mass movements and DSGSD is not well well-constrained (Bisci et al., 1996; Sorriso-Valvo et al., 1999), although the topographical modifications as well as the fractures, inherited and/or generated in a response to the DSGSD, must have a consequent impact. The knowledge of geomorphological evolution and massif fracturing due to DSGSD initiation and evolution is thus of primary importance to predict the locations of smaller mass movements.

This problem cannot be tackled by direct field observations alone for two reasons. The first one is that the large time scale involved in the process makes erosion and sedimentation efficient phenomena that mask the deformation of the mountain (Agliardi et al., 2001). The second one is that such a deformation seems to be very deep as geophysical survey is presently unable to determine the location of failure surfaces (Ferrucci et al., 2000).

* Corresponding author. Tel.: +33 492 94 26 20; fax: +33 492 94 26 10.
E-mail address: bachmann@geoazur.unice.fr (D. Bachmann).

0169-555X/$ – see front matter © 2008 Elsevier B.V. All rights reserved.
doi:10.1016/j.geomorph.2007.09.018

Using both 3-D experimental models and 2-D numerical models, we provide an accurate description of a synthetic DSGSD, especially regarding the morphological evolution and the deformation at depth. A 3-D physical modeling technique is used (Bachmann et al., 2004; Chemenda et al., 2005). Experimental models are performed in order to determine fracture location in the destabilization of a simple prismatic mountain. 2-D numerical models are also carried out to identify what are the rupture processes involved in DSGSD initiation.

2. Experimental set-up and procedure

The modeling technique is based on the use of an especially created "scaled" analogue material called Slope[1] and an original vertical accelerator device (Bachmann et al., 2004; Chemenda et al., 2005). The original vertical accelerator device consists of a mobile platform that can be uplifted up to 2 m and then released (Fig. 1). During free fall the platform reaches a maximum velocity of 6 m s^{-1}. It is then decelerated to zero velocity on a shock absorber. The model undergoes a strong acceleration (up to 500 m s^{-2}, Fig. 2) during this phase. Such an acceleration cycle is repeated several tens of time in order to obtain a well-developed macro deformation. Model deformation can be observed accurately after each acceleration cycle. This discrete loading technique has proved to be equivalent to a continuous quasi-static loading (Chemenda et al., 2005).

The used material Slope[1] has been developed to satisfy several similarity criteria. Among these the main criterion is (Shemenda, 1994):

$$\frac{\sigma_c^o}{\rho^o g^o H^o} = \frac{\sigma_c^m}{\rho^m g^m H^m} \quad (1)$$

where ρg is the specific weight (ρ is the density and g is the gravity acceleration, with $\rho^m = 0.86$), σ_c the strength under compression, H the spatial-scale of the phenomenon (the mountain height H, for example) and superscripts o and m mean original and model, respectively. The problem while developing scaled physical modeling materials is that the mechanical properties of the original material are not well known. In the case of rocks, a major unknown parameter is the friction angle. Indeed if the friction angle were similar at the mountain scale to that in a rock sample (generally between 20° and 40°, Hoek and Brown, 1997; Cruden, 2003), any mountain of common geometry (slope values of less than 40°) should remain stable. On the other hand the frictional strength decreases with an increase in temporal and spatial-scales, for various reasons (increasing amount of discontinuities, confinement conditions, creep mechanism activation, variations in pore pressure etc.). The friction angle at the mountain scale must therefore be very small, we thus decided to neglect this parameter. A more important parameter to take into account is the

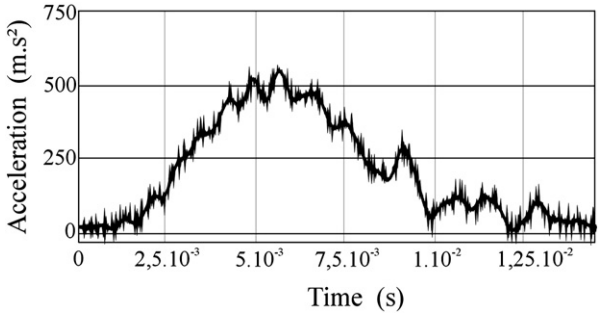

Fig. 2. Accelerogram by a high frequency accelerometer fixed to the mobile platform of the vertical accelerator shown in Fig. 1.

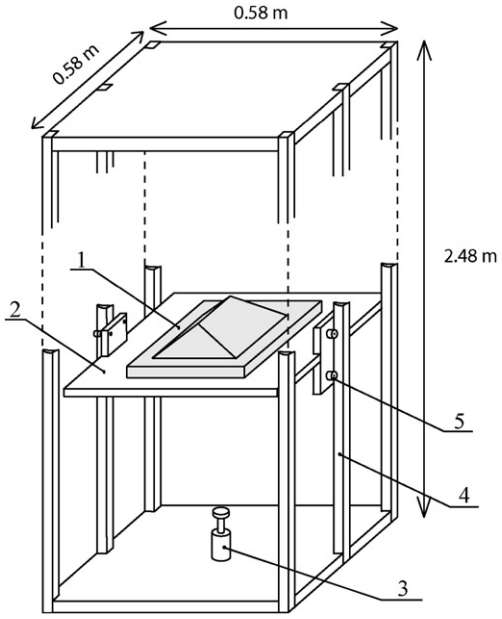

Fig. 1. Sketch of the vertical accelerator device designed to increase the "gravity force": 1) Model, 2) Mobile platform supporting the model, 3) Shock absorber, 4) Rails guiding the falling platform, 5) Ball bearings.

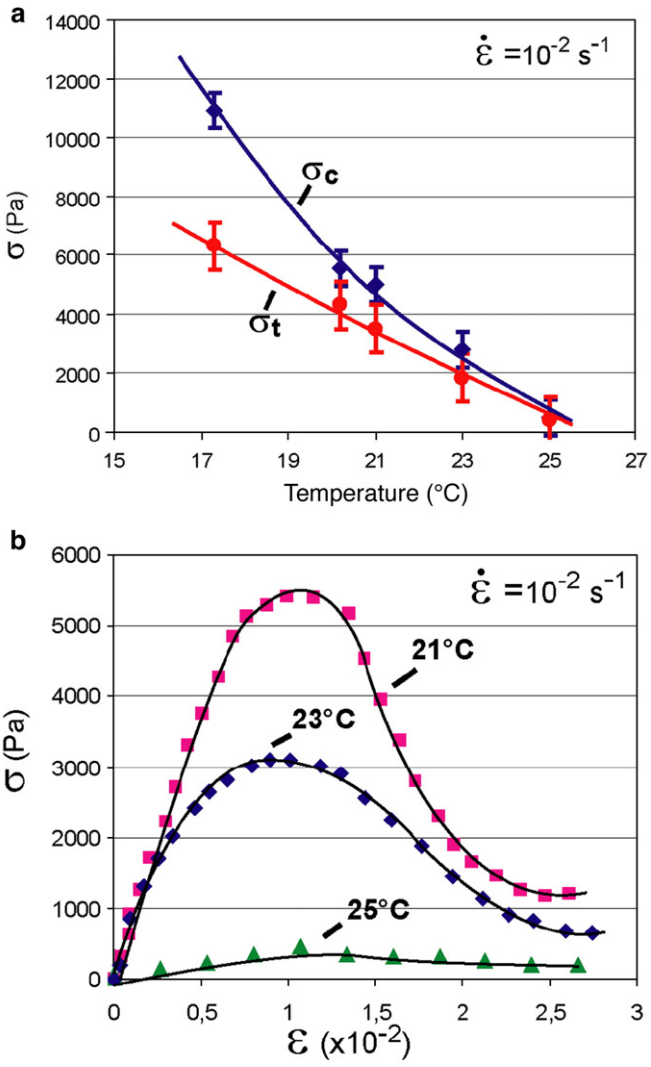

Fig. 3. Properties of the material Slope[1]. a) Compressive σ_c and tensile σ_t stress versus temperature, b) uniaxial stress/strain diagrams at different temperatures and constant strain rate $\dot{\varepsilon} = 10^{-2}$ s^{-1}.

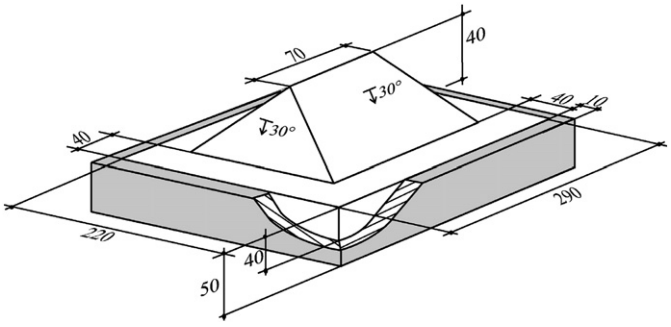

Fig. 4. Scheme of the model (dimensions are in millimeters). The model includes a prismatic mountain with all faces dipping at an angle of 30°, and a parallelepiped basement within a rigid box (strong coupling is ensured between the model and the box).

brittle behaviour of rock at shallow depth. This has been reproduced by using a material with strain softening. The material Slope[1] has thus a low frictional elasto-brittle-plastic behaviour with strain softening.

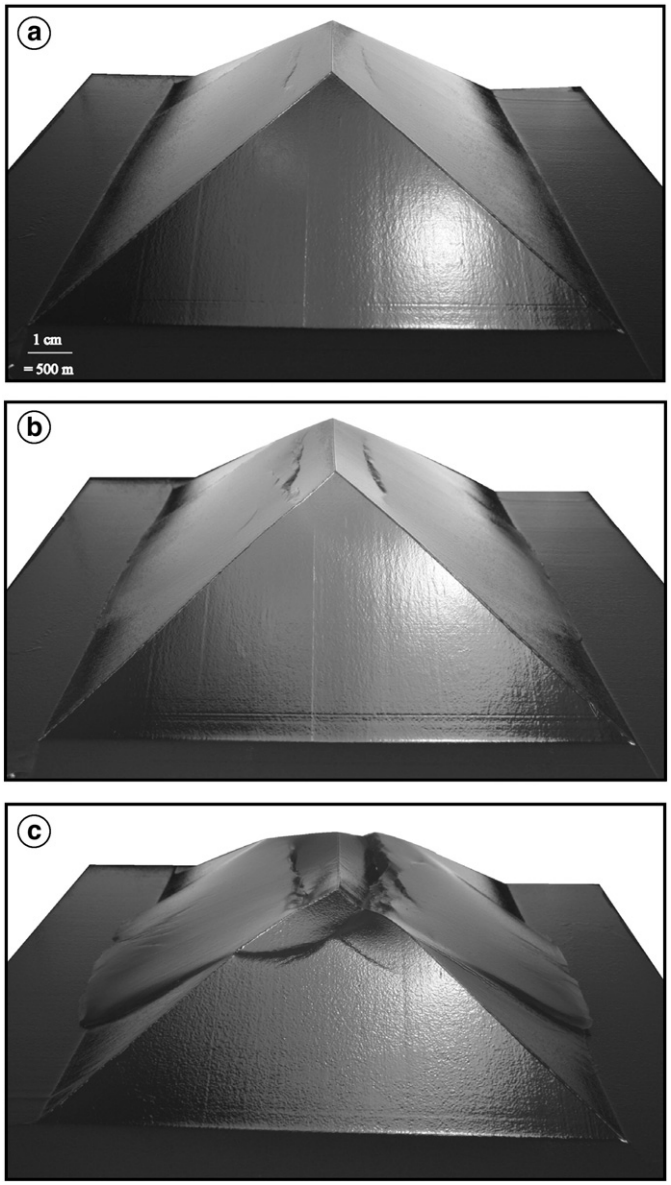

Fig. 5. Pictures presenting the failure of a model. (a) After 100 acceleration stages. (b) After 105 acceleration stages. (c) After 110 acceleration stages.

Its mechanical behaviour depends on the material composition, but also on the temperature and strain rate (Fig. 3). Variation of these parameters enables to obtain the needed material properties.

The experiments presented aimed to study the destabilization of a simple prismatic homogeneous mountain (Fig. 4). The model is made by pouring the melt of the material into a box. The material then crystallizes. It is then shaped to obtain the desired geometry. High coupling between the model and the box ensures no displacement at the model basement.

As in previous studies, we fixed the size of the model H^m and the strength σ_c^m of the analogue material by working at a constant temperature of 23 °C (σ_c^m=2800 Pa). A model was submitted to a series of acceleration cycles for a 250 m s^{-2} vertical "gravity" acceleration g^m. As no rupture occurred after more than a hundred acceleration cycles, another model was built and submitted to an increased g^m. The vertical ("gravity") acceleration g^m was thus increased step by step until failure was reached for about a hundred acceleration steps. The necessary vertical acceleration was of 400 m s^{-2}.

During an experiment, surface deformation is observed and registered using a high resolution digital camera. Morphological features are thus presented by using pictures. Cross-sections are made at the end of an experiment by cutting the model at various locations after cooling it to ca. 10 °C. Some experiments were stopped in the early stages of model deformation to analyze the corresponding internal deformation. Internal deformation is shown in cross-sections. In this last case, sketches are added to the pictures for a better description.

3. Experimental results

About 50 experiments have been performed, the most representative are presented below.

3.1. Experiment 1: Symmetrical deformation

3.1.1. Morphological evolution

The first evidence of fracturing of the model occurs after about a hundred acceleration steps for a 400 m s^{-2} acceleration. First fractures appear on the upper part of the two large sides of the model (Fig. 5a), parallel to the summit crest. Fractures are then observed at the base of both mountain sides (Fig. 5b). At this stage, we can observe the

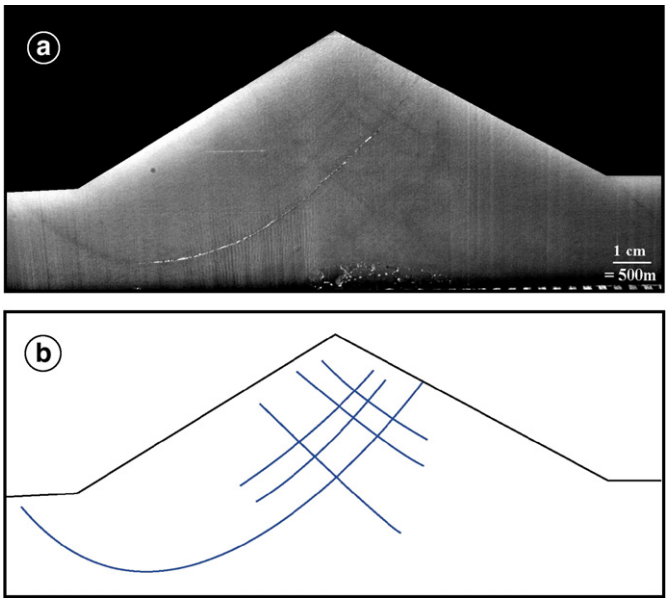

Fig. 6. Cross-section realized at an early stage of evolution (after 100 acceleration stages), in the middle of the model and perpendicular to the crest. (a) Picture of the section. (b) Sketch of the section.

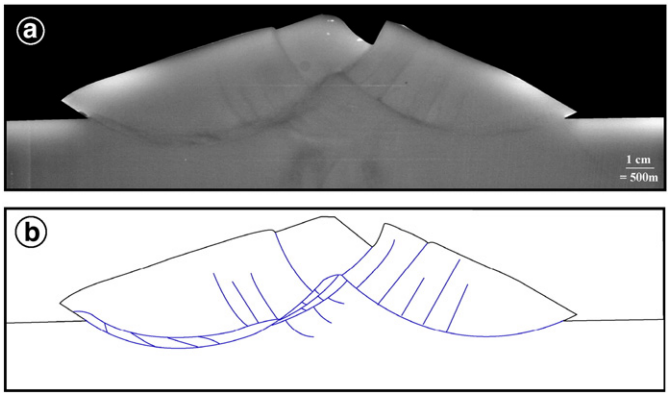

Fig. 7. Section A. Cross-section realized at an advanced stage of evolution for a symmetrical failure (after 110 acceleration stages), at an extremity of the crest and perpendicular to it. (a) Picture of the section. (b) Sketch of the section.

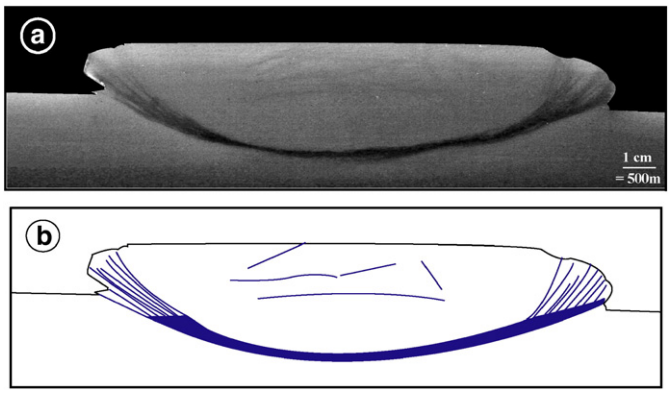

Fig. 9. Section C. Cross-section realized at an advanced stage of evolution for a symmetrical failure, parallel to the crest at the toe of the mountain. (a) Picture of the section. (b) Sketch of the section.

subsidence of the mountain top and a slight inflation of the mountain toe. Shear displacement increases then on the upper fractures and conducts the latter to propagate laterally through the two small sides (Fig. 5c). The intersection between the sliding masses and the topographic surface are clearly delimited. The two sliding masses involve almost the whole large sides. Their width at their base almost corresponds to the length of the summit crest. At the top they are wider, so that the lateral limits are curved. One of the slides develops more than the other. At the base of both sliding masses fractures are observed, intersecting each other in the middle of the lower limit of the slide. The summit crest gets curved, its centre sagging more than its extremities.

3.1.2. Internal deformation evolution

3.1.2.1. Initial stage of deformation. A vertical cross-section performed perpendicularly to the crest in the middle of the model is presented (Fig. 6). Six fractures are observed. Five of them are visible only inside the model and are shorter than the other, so that we can notice that fracturing initiates inside the model. The long fracture cross-cuts most of the model to delimit the sliding unit. This two long fracture reaches the topographic surface almost perpendicularly. In the lower part, the long fracture follows an almost circular trajectory. The maximum depth of the long fractures is of about the mountain height. This depth is reached under the lower third of the flank.

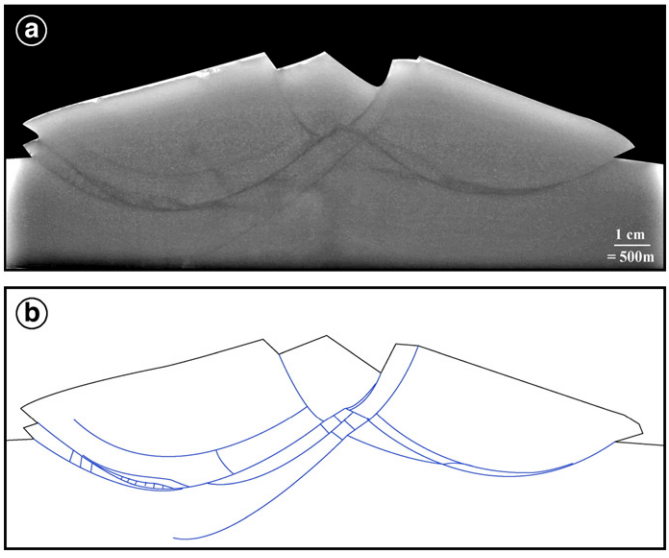

Fig. 8. Section B. Cross-section realized at an advanced stage of evolution (after 110 acceleration stages) for a symmetrical failure, in the middle of the model and perpendicular to the crest. (a) Picture of the section. (b) Sketch of the section.

3.1.2.2. Advanced stage of deformation. Three vertical cross-sections of the model are presented (Figs. 7–9). Two of them are perpendicular to the summit crest. One has been realized at one end of this summit crest (section A), and the other in the middle of the model (section B). The last cross-section (section C) has been realized, parallel to the summit crest, along the pre-failure slope toe.

Section A, Fig. 7: The two sliding units are clearly delimited at depth by a failure zone following an almost circular trajectory. The latter are composed of the long fractures forming in the early stages of the experiment but also of several fractures almost parallel to the first ones. The main failure zones correspond thus to a complex fracture network which becomes wider when the displacement of the sliding unit increases. This appears clearly in section A by comparing the two sides. The left hand side is indeed delimited at depth by a wider failure zone than on the other side, due to a more important motion. Several fractures perpendicular to the main failure zone are also observed. Most of them seem to correspond to the short fractures described in the initiation internal deformation stage. They develop upward and in some cases reach the topographic surface to form a counterscarp (section A on the right hand side).

Section B, Fig. 8: The two failure zones previously described are still observed. They are composed of several long fractures and of perpendicular shorter ones. The summit crest is located on a

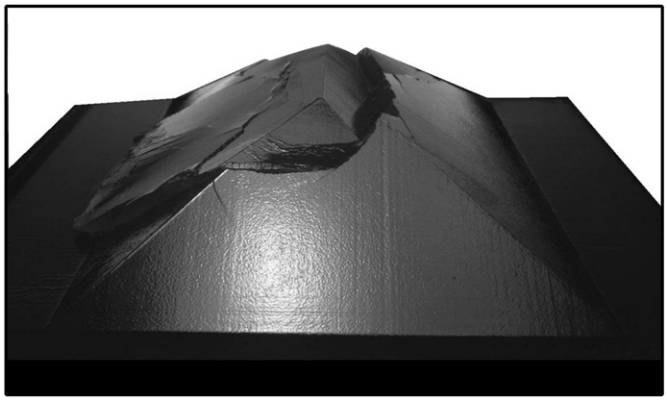

Fig. 10. Picture presenting the asymmetrical failure of a model after 110 acceleration stages.

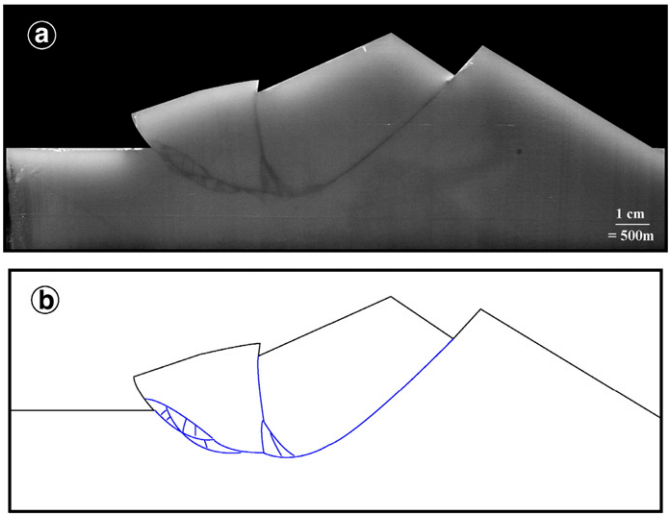

Fig. 11. Cross-section realized at an advanced stage of evolution (after 110 acceleration stages) for an asymmetrical failure, in the middle of the model and perpendicular to the crest. (a) Picture of the section. (b) Sketch of the section.

sagging wedge. The maximal thickness of the sliding mass is of about the mountain height.

Section C, Fig. 9: The main failure surface is curved. It is composed of several parallel fractures which diverge when they reach the topographic surface on both sides of the sliding unit. Few fractures are also observed near the surface in the centre of the sliding unit.

3.2. Experiment 2: Asymmetrical deformation

In some cases only one side of the mountain model is mobilized. The asymmetrical deformations represent about 30% of the experiments performed. The shape of the mobilized mass is almost similar to that of one of the sides failing in the symmetrical case (Fig. 10). A vertical cross-section realized perpendicularly to the crest (Fig. 11) shows that the failure is still located at a depth comparable to the mountain height. A major counterscarp is observed to accommodate the deformation, as do the other side's failure surface in the symmetrical case. It is vertical and located here at the lower third of the mobilized mass.

4. Numerical modeling

The purpose of this study is to reproduce physical modeling results to investigate the mechanical processes governing rupture initiation. To do this we used a 2-D finite element code named Adeli (Hassani, 1994), which has been especially created to study thermo-mechanical deformations in rock. The mountain has the same geometry and elasto-plastic rheology with strain softening, as in the above experimental models (Fig. 12). The cohesion of the material was of

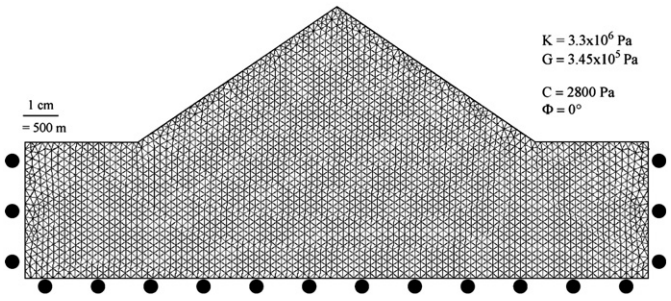

Fig. 12. Mesh and mechanical characteristics of the numerical model.

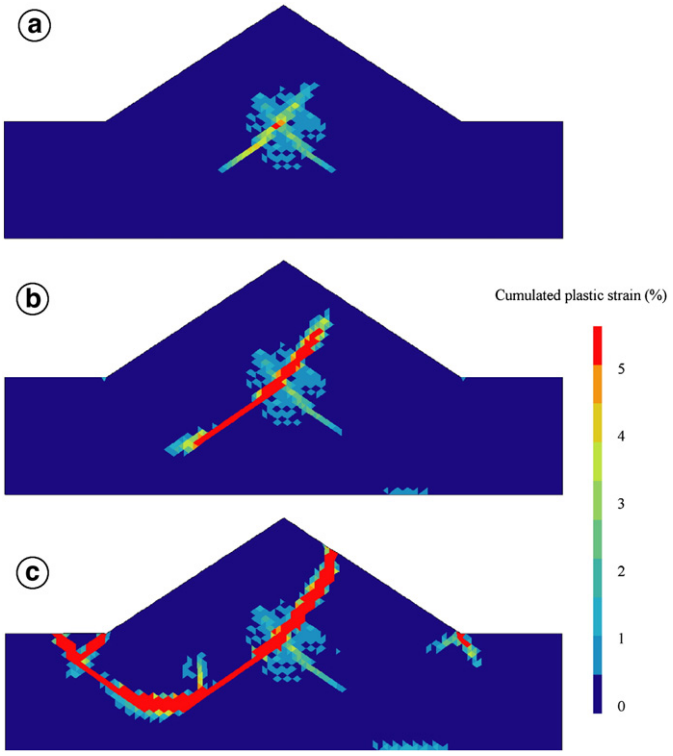

Fig. 13. Early stages of failure in numerical models.

2.8×10^3 Pa. This strength was reduced to 70% after a deformation of 0.01, as in the analogue material Slope[1]. The gravity acceleration was increased progressively (starting from $g^m = 0$ m s^{-2}), and then stopped when failure occurred.

Results show that the failure initiated for a gravity acceleration of 240 m s^{-2}. The failure (plastic strain accumulation) occurs inside the model (Fig. 13a). Two main localized plastic deformation zones are observed, dipping parallel to the two mountain sides, but only one of them develops (Fig. 13b). It generates a curved failure surface intersecting the slope almost vertically (Fig. 13c). At the toe of the slope it generates a wedge. Some plastic deformation is also observed at the toe of the slope which is not involved in the major slide. The thickness of the sliding unit almost corresponds to the mountain height.

5. Discussion and conclusions

Our experimental models provide new insights for a precise description of the DSGSD phenomenon, especially regarding morphological evolution, fracturing at depth and the mechanical behaviour of the rock mass at the mountain scale.

Our models reproduce well some of the morpho-structural features observed in nature, especially the sagging of the crest. Fracturing intersects the topographic surface near the crest almost perpendicularly, as in many DSGSD described in literature (Beck, 1968; Mahr and Nemcok, 1977; Savage and Varnes, 1987; Zanchi et al., 2002). In nature, however, more counterscarps are generally observed in comparison with our models. This is probably due mainly to the fact that pervasive fractures can pre-exist in the massif, and that these fractures can be reactivated by the gravitational movement (Radbruch-Hall, 1978; Hürlimann et al., 2006). Furthermore the failure surface observed in our models follows an almost circular trajectory. In nature such a simple shape should be influenced by the geological structure (Mahr, 1977; Agliardi et al., 2001; Zanchi et al., 2002; Ambrosi and Crosta, 2006). Some counterscarps should thus be generated as antithetic fractures in response to the motion if the failure surface is not as regular. Those pervasive fractures can also influence the whole

mountain destabilization (symmetrical versus asymmetrical). The asymmetrical deformations represent about 30% of the physical experiments performed. This should not happen in an ideally perfectly symmetrical model, but physical models as rock masses are never perfectly homogeneous.

Regarding the sliding surface, a striking aspect is that it is located at a maximum depth comparable to the mountain height. The similarity criterion Eq. (1) implies a link between this mountain height and the rock mass strength at the mountain scale. If we assume that the height of a mountain subject to DSGSD is H=2000 m, the rock mass strength at the mountain scale is σ_c^o=10 MPa. DSGSD are however observed even for much lower slope heights, of only a few hundred meters (i.e. ~200 m in Tibaldi et al., 2004). In this case the rock mass strength is also much lower (σ_c^o=10 MPa). Furthermore, the similarity criterion (Eq. (1)) shows that there are two possibilities for the triggering of a DSGSD: to reduce the rock strength at the mountain scale (that can be an effect of weathering or an increase in pore pressure), or to increase the slope height (that can be done by valley erosion for example). The threshold strength for the triggering of a gravitational destabilization should also be dependent of the slope gradient and shape, as well as by the structural settings and pattern of discontinuities. That should be studied in future work.

Both physical and numerical models show that the failure initiates inside the model. To our knowledge such behaviour has never been observed or proposed. Indeed some authors suggest that for homogeneous material failure should initiate at the crest of the slope (Romani et al., 1972; Chowdhury, 1978) or at the toe, where the higher shear stress is assumed (Veder, 1981; Zaruba and Mencl, 1982). Our models evidenced that the higher shear stress intensity, where failure initiate, is not located at the toe of the slope but inside the model below the crest. Regarding numerical modeling, we observe that it is an efficient tool for the modeling of the general aspect of the failure, at least in 2 dimensions. A whole side of the mountain is involved as in experimental models, and the depth of the failure surface still corresponds to the mountain height. It is however unable to reproduce the secondary fractures, and to tackle a large strain. In spite of this, numerical results show that rupture initiation in physical models is governed by Drucker–Prager criterion. The threshold acceleration to reach the gravitational failure is lower in the 2-D numerical models than in the 3-D experimental ones. Those differences can be due to the importance of a 3-D analyze of gravitational failure.

In nature, various mass movements of smaller extent are observed to be linked to DSGSD. Our results give some clues in order to understand this interaction. The fracturing of the massif is important during DSGSD evolution. Such a fracturing weakens the rock mass and facilitates water circulation and weathering. It is thus directly a preparing factor regarding gravitational mass movements. This seems particularly true along the fractures bounding the DSGSD. The rock mass is there pervasively fractured (see Fig. 9), so that debris-flows are highly facilitated in this zone, as observed in nature (Sorriso-Valvo et al., 1999). At the toe of the DSGSD, an unrealistic steepness of the slope is generated considering the time scale of those gravitational movements. Such steepness should be in nature compensated by shallow gravitational movements (Bisci et al., 1996). These smaller gravitational movements are however directly linked to precipitation and associated weathering and increased rock mass pore pressure which are not reproduced in our models.

References

Agliardi, F., Crosta, G., Zanchi, A., 2001. Structural constraints on deep-seated slope deformation kinematics. Eng. Geol. 59, 83–102.

Ambrosi, C., Crosta, G.B., 2006. Large sackung along major tectonic features in the Central Italian Alps. Eng. Geol. 83, 183–200.

Bachmann, D., Bouissou, S., Chemenda, A., 2004. Influence of weathering and pre-existing large scale fractures on gravitational slope failure: insights from 3-D physical modelling. NHESS 4, 711–717.

Beck, A.C., 1968. Gravity faulting as a mechanism of topographic adjustment. N.Z. J. Geol. Geophys. 11, 191–199.

Bisci, C., Burattini, F., Dramis, F., Leoperdi, S., Pontoni, F., Pontoni, F., 1996. The Sant'Agata Feltria landslide (Marche Region, central Italy): a case of recurrent earth flow evolving from a deep-seated gravitational slope deformation. Geomorphology 15, 351–361.

Chemenda, A., Bouissou, S., Bachmann, D., 2005. 3-D physical modeling of deep-seated landslides: new technique and first results. J. Geophys. Res. 110 (F4), F04004. doi:10.1029/2004JF000264.

Chowdhury, R.N., 1978. Slope Analysis. Elsevier, Amsterdam, p. 423.

Crosta, G.B., 1996. Landslide, spreading, deep seated gravitational deformation: analysis, examples, problems and proposals. Geogr. Fis. Din. Quat. 19, 297–313.

Cruden, D.M., 2003. The shapes of cold, high mountains in sedimentary rocks. Geomorphology 55, 249–261.

Ferrucci, F., Amelio, M., Sorriso-Valvo, M., Tansi, C., 2000. Seismic prospecting of a slope affected by deep-seated gravitational slope deformation: the Lago Sackung, Calabria, Italy. Eng. Geol. 57, 53–64.

Hassani, R., 1994. Modélisation numérique de la déformation des systèmes géologiques. PhD Thesis, Université de Montpellier II, France.

Hoek, E., Brown, E.T., 1997. Practical estimates of rock strength. Int. J. Rock Mech. Min. Sci. 8, 1165–1186.

Hutchinson, J.N., 1988. General Report: morphological and geotechnical parameters of landslides in relation to geology and hydrogeology. Proc. 5th Int. Symp. on Landslides. Lausanne, Balkema, Rotterdam, vol. 1 pp 3–35.

Hürlimann, L., Ledesma, A., Corominas, J., Prat, P.C., 2006. The deep-seated slope deformation at Encampadana, Andorra: a multidisciplinary approach. Eng. Geol. 83 (4), 343–357.

Kinakin, D., Stead, D., 2005. Analysis of the distributions of stress in natural ridge forms: implications for the deformation mechanisms of rock slopes and the formation of sackung. Geomorphology 65, 85–100.

Mahr, T., 1977. Deep-reaching gravittional deformation of high mountain slopes. Iaeg Bull. 16, 121–127.

Mahr, T., Nemcok, A., 1977. Deep-seated deformations in the crystalline cores of the tatry Mts. Iaeg. Bull. 16, 104–106.

McCalpin, J.P., Irvine, J.R., 1995. Sackungen at the Aspen Highlands ski area, Pitkin County, Colorado. Environ. Eng. Geosci. 1, 277–290.

McCleary, J., Dohrenwend, J., Cluff, L., Hanson, K., 1978. 1972 earthquake studis, Washington public power supply system Nuclear Projects Numbers 1 and 4. Woodward-Clyde consultants, San Francisco, 75 pp., unpublished report.

Radbruch-Hall, D., 1978. Gravitational creep of rock masses on slopes. In: Voight, B. (Ed.), Rockslides and Avalanches Natural Phenomena Developments in Geotechnical Engineering Eng., vol. 14. Elsevier, Amsterdam, pp. 607–657.

Romani, F., Lovell, C.W., Harr, M.E., 1972. Influence of progressive failure on slope stability. Jour. of the soil mech. and foundations division. Am. Soc. Civil Eng. 98, 1209–1223.

Savage, W.Z., Varnes, D.J., 1987. Mechanics of gravitational spreading of steep-sided ridges (sackung). Iaeg Bull. 3 (5), 31–36.

Shemenda, A.I., 1994. Subduction: insights from physical modeling. Mod. Approaches Geophys., vol. 11. Springer, New York. 215 pp.

Sorriso-Valvo, M., Gullà, G., Antronico, A., Tansi, C., Amelio, M., 1999. Mass-movement, geologic structure and morphologic evolution of the Pizzotto–Greci slope (Calabria, Italy). Geomorphology 30, 147–163.

Tabor, R.W., 1971. Origin of ridge-top depressions by large-scale creep in the Olympic Mountains. Soc. Geol. Am. Bull. 82, 1811–1822.

Tibaldi, A., Rovida, A., Corazzato, C., 2004. A giant deep-seated slope deformation in the Italian Alps studied by paleoseismological and morphometric techniques. Geomorphology 58, 27–47.

Veder, C., 1981. Landslides and their stabilization. Springer-Verlag, New-york, 247 pp.

Zanchi, A., Crosta, G.B., Stuletti, G., Sterlacchini, S., 2002. 3D geological modeling for slope stability problems. The case study of the Corno Zuccone sackung, Val Taleggio (Italy). Mem. Soc. Geol. Ital. 57, 585–594.

Zaruba, Q., Mencl, V., 1982. Landslides and their control. Elsevier, Amsterdam, Oxford. 324 pp.

Zischinsky, U., 1966. On the deformation of high slopes. Proc. 1st conf. Int. Soc/Rock Mech. Lisbon. Sect, vol. 2, pp. 179–185.